

Contents lists available at ScienceDirect

Acta Materialia

journal homepage: www.elsevier.com/locate/actamat





Shear-coupling of graphene grain boundaries: Elementary mechanisms, effects of topology, and role of buckling

Emil Annevelink^a, Brian Xu^a, Harley T. Johnson^a, Elif Ertekin^{*,a}

Department of Mechanical Science and Engineering, University of Illinois at Urbana-Champaign, Materials Research Laboratory, 104 South Goodwin Avenue, Urbana IL. 61801 USA

ARTICLE INFO

Keywords: Shear-coupling Grain boundaries Disconnections Out-of-plane deformations Graphene

ABSTRACT

Engineering grain boundary structure is a promising method for rational control of the microstructure and mechanical properties of two-dimensional materials. In bulk materials, shear stresses can drive grain boundary migration through the dislocations in grain boundaries. However, while shear coupling of grain boundaries has been studied in bulk materials like nanocrystalline copper, its translation to two-dimensional materials where out-of-plane deformation can relieve in-plane shear is not yet established. We investigate how the low flexural rigidity of graphene effects shear coupled grain boundary motion using atomic scale simulations of flat and buckled grain boundaries. We define the *coupling shear strain* as the strain at which a grain boundary has advanced by one Burgers vector and is at equilibrium and the *critical shear strain* as the strain at which migration of the first dislocation in the grain boundary becomes thermodynamically favorable. We show that the out-of-plane deformation does not influence the coupling shear strain and is governed only by the grain boundary topology. While the critical shear strain is altered somewhat by the low flexural rigidity due to buckling induced softening, it is also still dominated by the grain boundary topology. Our atomic scale results are synthesized into two models that predict the coupling and critical shears.

1. Introduction

The enhanced mechanical properties of nanocrystalline materials have spurred studies into their deformation behavior, many of which find that their plasticity is governed by stress-induced grain boundary migration [1–3]. Both experimental [1,4,5] and computational [6–8] studies suggest that this plasticity is based on shear coupling, in which shear strains promote the growth of one grain with respect to another, or equivalently, grain boundary migration results in shear of one grain with respect to the other. Many observed features of grain boundary motion, such as sliding [3,9], rotation [10,11], and stress-assisted growth [1], are compatible with the framework of shear coupling.

Shear coupling is based on the idea that the motion of a grain boundary intrinsically contains both perpendicular and parallel components [12]. The extent of coupling between shear strains and grain boundary motion across low to high angle grain boundaries can be described by the grain boundary's total dislocation content. This understanding of coupling is consolidated through a theory of disconnections – dislocations of the grain boundary itself – which are line defects lying within a grain boundary that can be characterized by a Burgers

vector and step height [13]. The motion of disconnections itself has been established as the elementary mechanism of shear coupling through investigations by Rajabzadeh et al. on bicrystalline copper [14]. This framework has been generalized to polycrystals by investigations of the nucleation and motion of grain boundary kinks and triple junctions [15–17].

The nanocrystalline grain structures exhibited by two-dimensional materials [18], that often result from the synthesis process, have prompted interest in understanding how grain boundaries migrate in lower dimensional lattices [19,20]. Recently, the dislocation-dislocation reaction mechanisms of grain boundary migration and their shear coupling have been identified for polycrystalline h-BN using transmission electron microscopy [11]. But no studies have yet addressed a primary difference between two-dimensional materials and their bulk counterparts. Two-dimensional materials have very low flexural rigidity and can deform out of plane [21]. In particular, shear can cause graphene sheets to exhibit out-of-plane wrinkling [22], and in graphene local out-of-plane deformation has been shown to alter dislocation-dislocation interaction energies by shielding long-range strain fields [23]. Since shear coupled migration is based on the

E-mail address: ertekin@illinois.edu (E. Ertekin).

^{*} Corresponding author.

framework of disconnections, and disconnections themselves have dislocation content, we expect that disconnection-disconnection interaction energies will be altered by out of plane deformation as well. Previously, the disconnection mechanisms of graphene grain boundaries were identified and a linear elastic theory was proposed to describe such disconnection-disconnection interactions [24]. However, neither shear coupling nor out-of-plane deformation was investigated as contributing factors to the grain boundary migration, even though it is reasonable to expect that shear coupled grain boundary motion may manifest differently in two-dimensional materials than in bulk materials. Here we will use the terms buckling and out-of-plane deformation interchangeably, in keeping with the terminology in the 2D materials literature.

While the effects of out-of-plane deformation, or buckling, on shear coupling in all 2D materials are generally of interest, we restrict ourselves to graphene as a prototypical 2D material whose mechanics and grain boundaries have been well studied [25,26]. We explore shear coupling in graphene in two separate regimes, one where the monolayer is constrained to be flat and another where it is free to buckle out-of-plane. These regimes represent two limiting extreme environments for graphene: either sandwiched between other constraining layers (as in a layered stack of h-BN for isolation) [27] or freestanding (as in a mechanical resonator) [28]. Studying grain boundary migration in two-dimensional materials may help to generally better understand their mechanical response, as well as to better learn how grain boundary structure evolves in order to ultimately control it [29].

2. Computational methods

The shear coupling of grain boundaries in graphene is investigated using atomic scale simulations as implemented in the software package LAMMPS [30]. The energies of the graphene supercell configurations are described by the reactive force field ReaxFF [31,32] as parameterized by Srinivasan et al. for condensed phases of carbon [33]. ReaxFF was chosen as it has been shown to capture energy variations arising from curvature and can model bond breaking and formation during dislocation movement [31,32]. Moreover, the potential energy land-scape of ReaxFF is smooth during bond order changes, which allowed us to investigate transition barriers and overcome spurious local minima (see below) using the nudged elastic band (NEB) method [34,35].

Graphene supercells are constructed with two grain boundaries of opposite orientation according to a Voronoi tesselation algorithm developed by Shekhawat et al. [36,37]. A schematic of a supercell with two anti-parallel grain boundaries is shown in Fig. 1, where the width W is given by twice the grain boundary separation d_{gb} . The supercell is tiled in space and is subject to periodic-boundary conditions in the xy plane and free boundary conditions in the z-direction. The supercell height H is a function of the grain boundary misorientation angle θ and the number of times that the primitive cell – each containing one dislocation per grain boundary – is repeated in the vertical direction. The number of primitive cell repeats is reported by the dimensionless parameter \overline{H} , where the height H is normalized by the primitive supercell height as defined by the grain boundary crystallography. We focus on zig-zag grain boundaries [26] that have only a single dislocation per primitive cell. The shear coupling is investigated for varying misorientation angles and supercell heights, with grain boundary separation d_{gb} large enough that the intra-grain boundary disconnection energy dominates the inter-grain boundary interaction. Following the scaling analysis in our previous work [24], we choose a supercell width W of 200 Asuch that there is no disconnection interaction between the two grain boundaries.

Using the constructed supercells, we migrate one grain boundary per supercell by moving one dislocation at a time until the whole grain boundary has shifted by one burgers vector. This gives all the intermediate configurations and energies for grain boundary migration. The migration is shown for a small supercell with two dislocations $(\overline{H}=2)$ per grain boundary in Fig. 1. For supercells with two dislocations per

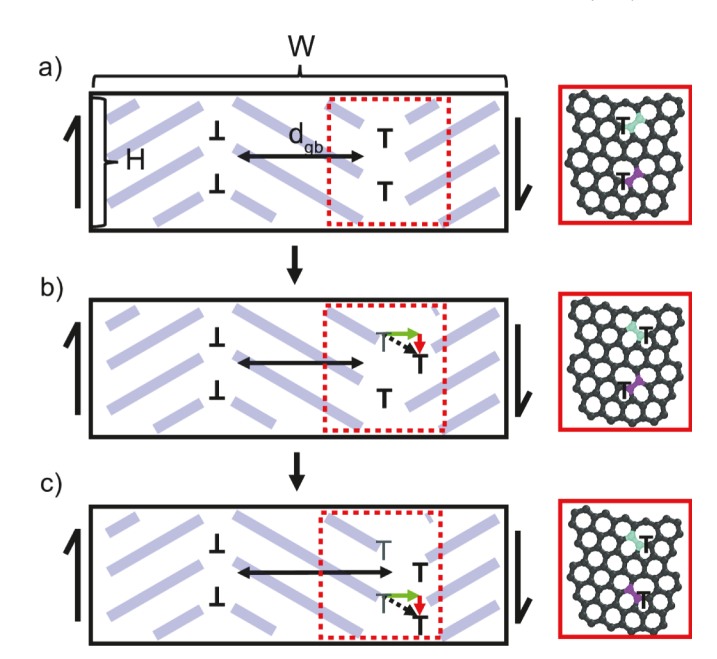


Fig. 1. Schematic of a representative supercell for shear coupling simulations. Three configurations (panels a, b, and c) show the stages of grain boundary migration. For each configuration, the atomic scale configuration of the grain boundary (inset in red) and a macroscale schematic of the supercell are given in which the red dashed lines denote the location of the atomic scale image. Each supercell contains two antisymmetric grain boundaries. In the panels, as the upper grain boundary migrates, it moves between (a) straight to (b) kinked and back to (c) straight. The migration occurs through 90° bond rotations of the grain boundary dislocations, where the cyan bond rotates to transform (a) to (b) and the magenta bond rotates to transform (b) to (c). The red and green arrows in (b,c) show the step and dislocation content of dislocation migration. (For interpretation of the references to color in this figure legend, the reader is referred to the web version of this article.)

grain boundary, there are three states corresponding to a straight, kinked, and straight grain boundary. The states are indexed using the reaction coordinate *RC* of migration, which tracks the degree to which the grain boundary has migrated. The reaction coordinate is determined according to the ratio of dislocations migrated. The reaction coordinates are RC: 0, RC: 0.5, and RC: 1 for the grain boundaries in Fig. 1(a,b,c) respectively. Both RC: 0 and RC: 1 correspond to supercells with straight grain boundaries, but for which the sizes of the grains differ. For a rectangular (unsheared) supercell, this causes the energy of RC: 1 to be slightly higher than that of RC: 0 due to the built-in shear from different sized grains. Alternatively, if the supercell vectors were allowed to relax they would develop a shear, and then the energy of RC: 1 would be equal to the energy of RC: 0 with a rectangular supercell. This coupling shear corresponds directly to the shear-coupled grain boundary motion that will be investigated below.

The supercell construction and grain boundary migration procedure described above results in graphene configurations that are flat. Identifying the lowest energy buckled configurations proved to be numerically challenging due to the large number of distinct but energetically nearly degenerate buckled configurations corresponding to each intermediate stage of grain boundary migration. For instance, relaxing the same topology (same kinked grain boundary) from slightly different initial out-of-plane perturbations often resulted in slightly different final geometries and energies. We found that damped dynamics minimizers like FIRE [38] do not find consistent local minima, so a different approach was needed to identify the lowest energy configurations. We adopted an iterative process where grain boundaries were first perturbed out-of-plane and relaxed and then NEB calculations of bond rotations were used to explore nearby minima. This admittedly unconventional use of NEB arose when, while investigating energy

barriers (transition states) for dislocation migration, we realized that NEB could simultaneously be used to effectively identify lowest energy intermediate configurations of grain boundary migration.

To explain the NEB procedure we developed further, consider the grain boundary migration shown in Fig. 1, for which the metastable intermediate configurations are associated with RC: 0, RC: 0.5, and RC: 1. A transition pathway is present between RC: $0 \rightarrow RC$: 0.5, and another between RC: $0.5 \rightarrow RC$: 1. Two NEB calculations should then be carried out, one for each transition. These two transitions and their energy profiles compose a "chain of NEB simulations" between successive intermediate configurations of grain boundary migration. For each individual NEB simulation, the mechanism to migrate a dislocation is a 90° rotation of the bond connecting two carbon atoms in the heptagon that makes up the edge dislocation [39,40]. In the atomic scale schematics of Fig. 1, the bonds that rotate are colored in teal and magenta. To obtain the buckled transition pathways, each of the two NEB replicas is initialized such that the bond rotates with an out-of-plane component. In this way, the use of the successive chain of NEB calculations constrains the explored configurations to those that would be passed through as a grain boundary advances by one Burgers vector. However, we found that the individual NEB simulations would often obtain intermediate images with lower energy than the initial/final states. The iterative NEB process consists of updating the initial/final configurations to nearby lowest energy states identified by the previous iteration. The iterative process concludes once smooth NEB trajectories between consistent initial and final states, for complete migration of the grain boundary, is achieved. Further details on the implementation of the iterative algorithm and an example can be found in the SI.

We note that the original intended use of the NEB calculations was to find the energy barriers associated with each dislocation migration. However, in the following the NEB results are used only within the iterative method to obtain robust intermediate configurations (the transition state barriers themselves are not discussed further). For completeness, these barriers are reported more thoroughly in the SI; we find that they do not change/alter any of the subsequent analysis.

3. Results

Shear coupling is investigated by exploring the energy landscape of each intermediate configuration by applying shear, and comparing the relative energies. Shear is applied through a displacement boundary condition parallel to the grain boundaries as depicted by the arrows to the left and right of the supercells in Fig. 1. Shear coupling can be understood by considering the disconnections that are present in the grain boundary (which themselves arise when different numbers of dislocations have migrated). Disconnections have both a dislocation character and a step height, and it is the dislocation content that gives rise to the shear coupling [41]. Given a particular grain boundary there are many different disconnection modes that can be activated. In the real world this causes complex behaviors and even dependence on temperature [42–44]. In our case, we limit our analysis to grain boundary migration where the 5|7 dislocation migrates by one lattice vector. In graphene, this limits the available disconnection modes to three, two climb modes and one glide mode. We take the glide mode as the lowest energy mode since it does not require diffusion of carbon atoms. The glide mode corresponds to the above reported algorithm for dislocation migration based on bond rotation so that only a single disconnection mode is activated.

The activated disconnection has a dislocation content and step height shown in Fig. 1(b,c) using red and green arrows respectively. The grain boundary coupling factor β is defined by the ratio of these two quantities according to

$$\beta = \frac{|\overrightarrow{b}|}{|\overrightarrow{s'}|} , \tag{1}$$

where \overrightarrow{b} is the disconnection Burgers vector and \overrightarrow{s} is the disconnection step height. The coupling factor highlights that as a grain boundary migrates, it not only moves perpendicular to the line of the grain boundary but also parallel. The parallel movement of a grain boundary – the dislocation content of a disconnection – underpins shear coupled grain boundary migration.

The coupling factor for graphene grain boundaries is determined by the disconnection modes that are active. The coupling factor will be measured later through the coupling shear. Here we start by defining the coupling factor using crystallography. Since only a single mode is active, we can define the coupling factor directly based on the single active disconnection using the grain boundary misorientation angle θ . Rather than expressing the coupling factor in terms of misorientation angle θ , it is more straightforward to use the coincidence site lattice (CSL) parameter Σ , which exhibits a one-to-one mapping to the misorientation angle [45,46]. The coupling factor, in terms of Σ , is given by

$$\beta = \frac{\sqrt{\Sigma}}{(\Sigma - 1)} \quad . \tag{2}$$

As we increase Σ (decrease θ) we reduce the coupling factor until we reach the limit of an isolated dislocation that has zero shear coupling normal to its Burgers vector.

We compare this predicted coupling factor to the measured coupling shear by applying a shear (fixed displacement boundary condition) to our supercells. Fig. 2 shows the variation of the energy with applied shear for a $\theta=21.8^\circ$ (Σ 7) grain boundary for the three states defined in Fig. 1 with W=200 Å and $\overline{H}=2$ for a flat supercell. The energies and strains are referenced to the unsheared supercell at RC: 0. The blue curve shows the energy for RC: 0, which increases monotonically from zero at zero applied shear. The green curve corresponds to RC: 1, which initially decreases, reaches a minimum at an applied shear of 0.46%, and then increases with additional shear. As shear is applied, the relative energies of the states change since the applied strain compensates for the residual strain of the moving grain boundary. Therefore, while RC: 0 has the smallest energy initially, the energies of RC: 0 and RC: 1 are equal at a strain of 0.23% from which point RC: 1 always has a lower energy, implying that the fully migrated grain boundary is thermodynamically

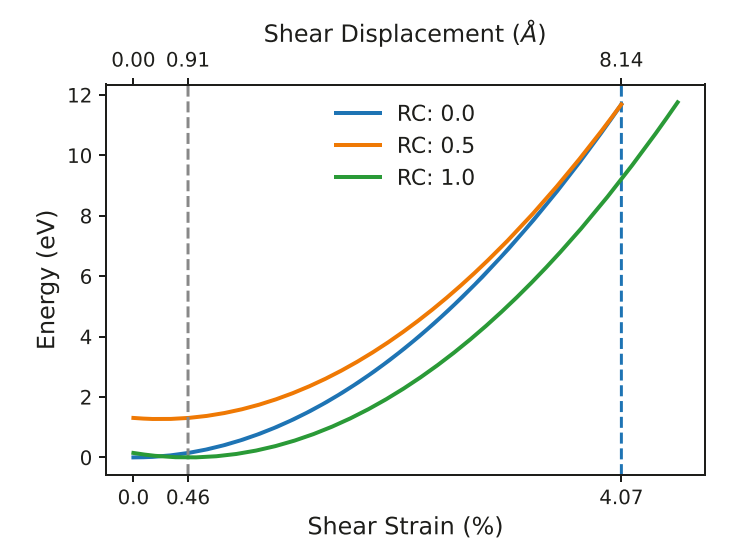


Fig. 2. The shear energies of the states for a flat supercell with $\overline{H}=2$ as defined in Fig. 1. Labels RC: 0, 0.5, 1 correspond to the configurations shown in Figure 1 (a,b,c) respectively. The vertical gray dotted lines at shear strains of 0.46 and 4.07 respectively correspond to the coupling shear strain of the migrated boundary (RC: 1) and the critical strain at which the energy of the partially migrated boundary (RC: 0.5) and the initial configuration (RC: 0) become equal.

favorable. We refer to the shear at which the minimum appears for RC: 1 as ε_{coup} , the coupling shear caused by migrating a grain boundary by one Burgers vector. The coupling shear is directly related to the relative displacement of the two grains as will be discussed more below. For this supercell ($\theta=21.8^{\circ}$, $\overline{H}=2$) the coupling shear is 0.46% shear strain. For reference, we also include the absolute displacement in the figures as a reference to compare the magnitude of the coupling Burgers vector. For this supercell, we measure a coupling Burgers vector magnitude of 0.91 Å.

In Fig. 2, the orange curve corresponds to RC: 0.5, the configuration with a disconnection present. This curve decreases initially to its minimum value at 0.23% before increasing. By comparison of RC: 0.5 and RC: 1 at zero applied shear, the disconnection energy for RC: 0.5 (essentially, the energy to introduce two disconnections with opposite Burgers vector) is much greater than the energy coming from the residual shear strain for RC: 1. As shear is applied, the energy of RC: 0 becomes equal to RC: 0.5 at a relatively large shear of 4.07%. Imagining the migration of the grain boundary occurring in two steps from RC: $0 \rightarrow RC$: 0.5 and then RC: $0.5 \rightarrow RC$: 1, the first transition becomes favorable at a relatively large shear of 4.07%, after which the second transition is already energetically favorable (0.23%). The critical value of the shear at which this particular sequence for GB migration is thermodynamically favorable is therefore given by the limiting value of 4.07%, associated with the intermediate configuration.

For this example, since $\overline{H} = 2$, RC: 0.5 is the only intermediate configuration in our supercell between the original and migrated boundary. For larger \overline{H} , there would be additional intermediate steps as each subsequent dislocation migrates, and each of these intermediate configurations would be associated with a particular degree of shear at which the intermediate configuration becomes favorable compared to the previous one. Amongst all of these transitional shears, we label the largest one as the *critical shear* ε_{crit} , the shear at which all subsequent intermediate configurations are equal or downhill in energy. Although the complete migration of the straight grain boundary (RC: 1) is favorable at a modest shear, the intermediate states have higher energies and require larger shears to become favorable. Curiously, it is always the first intermediate state, the one that transforms the straight grain boundary into one with disconnections, that determines the critical shear of migration. The critical shear is therefore the strain at which the energy of a grain boundary with one migrated dislocation, corresponding to the smallest disconnection length possible (RC: $1/\overline{H}$), is equal to the energy of sheared RC: 0 configuration. For the case of two dislocations ($\overline{H}=2$) in Fig. 2, ε_{crit} corresponds to the case in which E(RC: 0) = E(RC: 0.5), but for supercells with three dislocations ($\overline{H} = 3$), to the case in which E(RC): 0) = E(RC: 0.33). After the critical shear, subsequent intermediate states all have lower energies and migration becomes thermodynamically favorable for all intermediate stages up to the straight grain boundary RC: 1. Together, ε_{coup} and ε_{crit} enable quantitative comparison of the shear coupling of graphene grain boundaries across misorientation angles and supercell heights and will be used to determine the role of out-of-plane deformation.

3.1. Misorientation angle dependence of shear coupling

Fig. 3 shows the coupling shear and the critical shear, reported for various Σ to highlight trends in shear coupling across misorientation angles for both flat and buckled supercells. The four investigated misorientation angles are $\theta=21.8^{\circ},13.1^{\circ},9.43^{\circ},4.83^{\circ}$, corresponding to $\Sigma 7$, $\Sigma 19$, $\Sigma 37$, $\Sigma 127$ respectively. In Fig. 3 each of the supercells have W=200 Å and $\overline{H}=2$.

The coupling shears for both flat and buckled supercells are plotted in Fig. 3(a). The flat and buckled configurations have identical coupling shears, implying that this quantity is independent of out-of-plane relaxation. This indicates that, like in bulk materials, shear coupling is a topological quantity that is essentially governed by the nature of the grain boundary. It is unaffected by local relaxations such as out-of-plane buckling. This result can be understood with the definition of shear coupling as the relative displacement that a grain boundary makes parallel to its line direction, while out-of-plane deformation to relieve the local strain around the dislocation core. Importantly, the out-ofplane deformation does not change the dislocation content around any of the dislocations. Therefore, while the out-of-plane deformation relieves energy of the grain boundary, it does not change the parallel motion of the grain boundaries and therefore does not change the shear coupling. Accordingly, we propose a simple analytical model to describe the dependence of the coupling shear on the grain boundary topology according to

$$\varepsilon_{coup} = \frac{|\overrightarrow{b}_{coup}|}{W} = \frac{a_{gr}}{\sqrt{\Sigma}W} , \qquad (3)$$

where $\overrightarrow{b}_{coup}$ is the Burgers vector of the disconnection dislocation, W is the grain boundary width, and a_{gr} is the lattice constant for graphene. The model is compared against the coupling shear as calculated by LAMMPS in Fig. 3(a) using a red line. The model reproduces the minimum shear for the four supercells considered for both flat and buckled configurations, further supporting the topological nature of shear coupling. The agreement between our model (Eq. 3) and atomistic

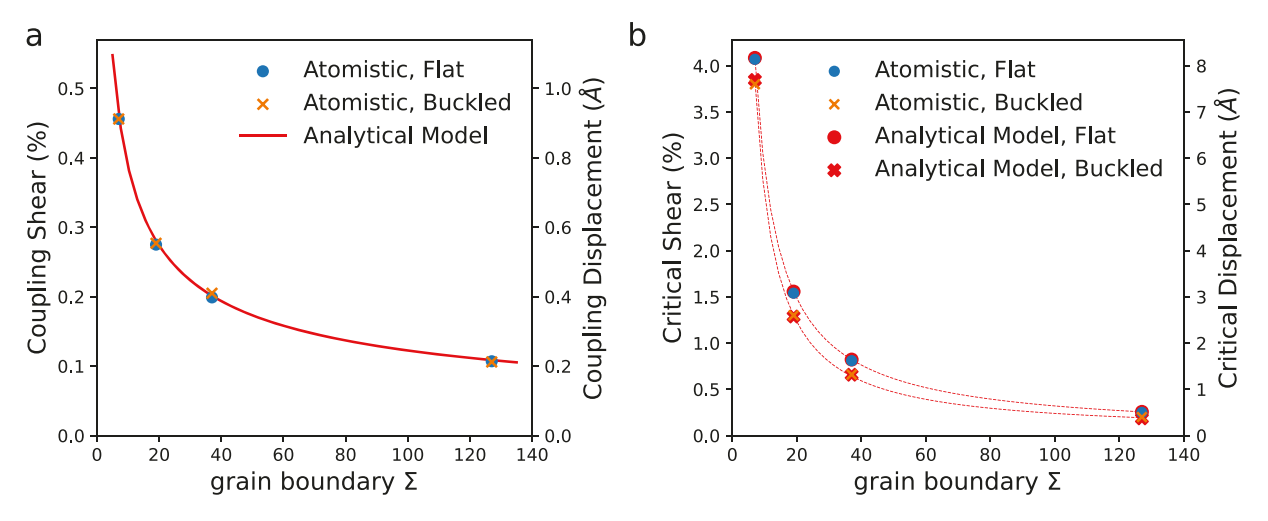


Fig. 3. The (a) coupling shear and (b) critical shear versus the grain boundary dislocation density Σ for both flat and buckled supercells. Model predictions are shown in red. (For interpretation of the references to color in this figure legend, the reader is referred to the web version of this article.)

simulation shows that the relative displacement of the grains is readily predicted by crystallography, validating the coupling factor given in Eq. 1. In particular, the strain that was originally accommodated by shearing the grains is completely relaxed when the disconnection Burgers vector is the displacement boundary condition in our simulation.

By contrast, we find that the critical shear is somewhat altered by out-of-plane relaxation. Fig. 3(b) shows the critical shear strain vs. Σ . Although the buckled and flat curves no longer lie on top of each other, the difference between the two curves remains fairly modest. Compared to the flat supercells, the critical shears of the buckled supercells are reduced by at most 0.3% strain, which is observed for the $\theta=21.8^{\circ}$ (Σ 7) grain boundary. With increasing Σ , the difference in critical shear decreases, signifying that buckling has less and less total impact on the critical shear for low angle (high Σ) grain boundaries.

To understand the difference of critical shear with respect to topology and out-of-plane deformation, we introduce another analytical model. In this case, the buckling dependence is directly included by utilizing the energies at zero strain for the first intermediate configuration relative to the straight grain boundary, E_{RC1} . The critical shear dependence is modeled according to

$$\varepsilon_{crit} = \frac{E_{RC1}\sqrt{\Sigma}}{(RC_1)a_{gr}\mu H} , \qquad (4)$$

where (RC_1) is the reaction coordinate of the first intermediate state, μ is graphene shear modulus, and H is the supercell height. A full derivation of the model, based on setting the energies of RC: 0 and RC: $(1/\overline{H})$ as a function of shear equal to each other, is available in the SI. A key assumption of this model is that the shear response of both the straight and the kinked grain boundary follow linear elasticity, allowing the use of the shear modulus to map the critical strain back to the zero strain energy.

To clarify the application of the model in Eq. 4, the parameters that appear on the right hand side are first determined and then used to predict ε_{crit} . The predicted ε_{crit} is then compared to the value obtained from atomistic simulations. Amongst the parameters that appear on the right hand side, all are geometric (set by the grain boundary topology) except for shear modulus μ and E_{RC1} . E_{RC1} itself is obtained from atomistic simulations. The shear modulus is obtained for each supercell by fitting to energy vs. shear plots (e.g. Fig. 2). For flat, pristine graphene (no grain boundaries) we find $\mu = 2.65$ eV/Ų, similar to others reported in the literature [40]. As discussed in the next section, in some instances when the supercells deform out-of-plane, the value of μ may vary; this parameter therefore represents an effective shear modulus, accounting for the effect of out-of-plane deformation on the energy required to shear the material.

The model predictions are plotted in Fig. 3(b) for each grain boundary in red. As opposed to the continuous prediction in Fig. 3(a), those in Fig. 3(b) are discrete since we rely on the computed atomistic value of the energy E_{RC1} of the discrete grain boundaries (the dashed red lines are shown as a guide). The comparison shows that the difference in critical shears for flat and buckled cases is almost fully accounted for by the out-of-plane relaxation, validating our model. Finally, we note that although we use energies E_{RC1} from atomistic calculations, the energy could also be obtained from a continuum dislocation model for disconnections that accounts for out-of-plane relaxation, allowing for faster determination of the critical shear of migration [23].

3.2. Effect of finite supercells on shear coupling

The simulations presented here invoke periodic boundary conditions, for which finite size effects and image interactions may be present. In order to determine the effect of the finite supercells and to gain an understanding of the shear coupling behavior for more realistic grain boundaries, we consider the dependence of the critical shear on the supercell height \overline{H} . For this analysis, we limit ourselves to the higher

angle grain boundaries of $\theta=21.8^\circ$ and $\theta=13.1^\circ$ as the number of atoms becomes large for the lower angle grain boundaries. In addition, the dependence of the coupling shear is not further considered because it depends only on the misorientation angle and is independent of the supercell height.

The dependence of the critical shear versus normalized height is plotted in Fig. 4(a). The critical shear is reported for $\overline{H}=2$, the smallest possible supercell size that can form a disconnection, up to $\overline{H}=10$. The atomistic results are plotted as circles/squares while the analytical model for the critical shear from Eq. 4 is plotted as solid/dotted lines for flat/buckled supercells. The results from atomic scale calculations shown in Fig. 4(a) generally agree with the predictions of the critical strain model from Eq. 4. While the model properly captures trends across the full set of systems considered, there are some differences for the buckled cases particularly for $\theta=21.8^\circ$.

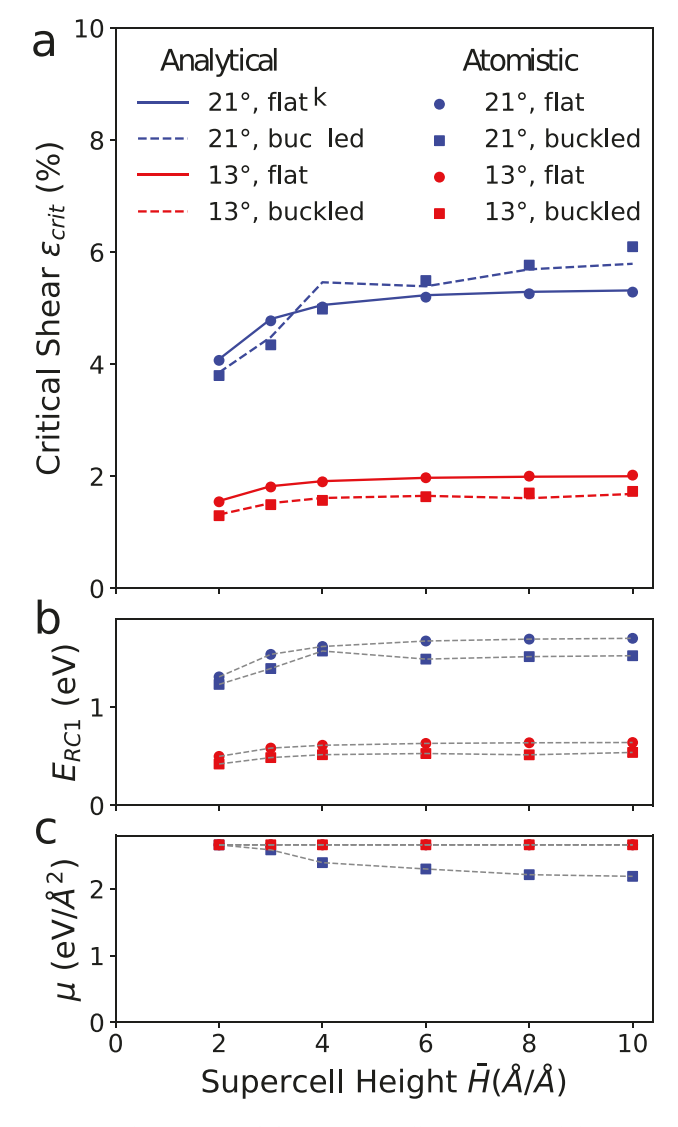


Fig. 4. Dependence of critical shear on supercell size. (a) Critical shear versus reduced supercell height \overline{H} for flat and buckled supercells containing 21.8° or 13.1° grain boundaries. The atomistic results are plotted as circles (squares) for flat (buckled) configurations respectively, and the critical shear model is shown by solid (dotted) lines for flat (buckled) configurations respectively. The isolated contributions to the critical shear model from the disconnection energy and the shear modulus are shown in (b,c) respectively. In (c), the shear moduli of 21° flat, 13° flat, and 13° buckled are nearly identical, which is why only 13° buckled is visible. In (b,c), the gray dotted lines are a guide to the eye for the atomistic contributions.

Starting with the flat supercells, the critical shear dependence for both $\theta=21.8^\circ$ and $\theta=13.1^\circ$ on \overline{H} shows a similar behavior in which it initially increases and then reaches a plateau by $\overline{H}\approx 8$. Moreover, the previous analytical model in Eq. 4, shown via the solid lines, captures the dependence for both grain boundaries. For reference, the model inputs – the energy of the first intermediate state and the effective shear modulus – are plotted in Fig. 4(b,c). For the flat cases, E_{RC1} has a similar trend to the critical shear in Fig. 4(a). In addition, we can see that μ is constant and equal to its value in pristine graphene ($\mu=2.65~{\rm eV/\mathring{A}^2}$).

The dependence of the critical shear versus supercell height for the buckled configurations is not as straightforward. For $\theta=13.1^\circ$, the same trends hold as for the flat case. The critical shear for buckled grain boundaries with misorientation angles of $\theta=13.1^\circ$ plateau at $\overline{H}\approx 6$. The constant offset between the buckled and flat cases for $\theta=13.1^\circ$ arises from a fixed reduction in the disconnection energy, as out-of-plane buckling reduces the energy of the disconnection core by a finite amount. The value of the effective shear modulus remains $\mu=2.65$ eV/ Ų. However, the critical shear for buckled grain boundaries with $\theta=21.8^\circ$ shows a more complex behavior. Instead, the atomistic results show that the critical shear for buckled $\theta=21.8^\circ$ (blue squares) crosses and then becomes larger than the flat critical shear (blue circles). This crossing occurs despite the disconnection energy being reduced by buckling, as seen in Fig. 4(b), similar to $\theta=13.1^\circ$.

The different behavior for buckled $\theta = 21.8^{\circ}$ stems from shear softening, as shown by the effective shear modulus in Fig. 4(c). The shear modulus is observed to slightly drop from $\mu = 2.65 \text{ eV/Å}^2$ as the supercell height increases. If the $\theta=21.8^{\circ}$ analytical model was plotted with the same shear modulus as the flat case, the buckled model would also show a plateau with a regular offset below the flat system just like the offset for $\theta = 13.1^{\circ}$. According to Eq. 4, for the analytical model to be able to reproduce the crossing behavior, it is necessary for the effective shear modulus to change. The softening of the shear modulus effectively accounts for the breakdown of linear elasticity due to the out-of-plane deformation and the induced curvature. It is reasonable that the effective shear modulus decreases as wrinkles form, since linear elasticity no longer holds and higher order terms like bending play a role. We suspect that if we continue to increase the supercell size, the $\theta = 21.8^{\circ}$ buckled shear moduli and therefore the critical shear would also plateau, albeit at a higher critical shear than the flat case.

3.3. Misorientation angle dependence of shear softening

The difference in critical shears for the two buckled grain boundaries stems from different buckling modes. As has been observed previously, while the low angle straight grain boundaries are buckled, the high angle $\theta=21.8^\circ$ grain boundary of graphene remains flat even when unconstrained [25]. This difference is reflected clearly in the atomic scale structures shown in Fig. 5, which shows that for straight (RC: 0 and RC: 1) grain boundaries, $\theta=13.1^\circ$ show out of plane corrugation at roughly a height of 2 Å (Fig. 5(d,f)) while $\theta=21.8^\circ$ show no corrugation (Fig. 5(a,c)). Interestingly, however, when a disconnection is introduced, both $\theta=21.8^\circ$ and $\theta=13.1^\circ$ grain boundaries are buckled. The change in the degree of buckling between the flat and disconnected grain boundary is much more pronounced for $\theta=21.8^\circ$. The buckling for $\theta=21.8^\circ$ at RC: 0.5 has a distinct sinuous character, with positive and negative out of plane displacements. This is distinct from $\theta=13.1^\circ$, where the out-of-plane displacements all lie in the same direction.

We believe that this different buckling behavior is responsible for the softening of the effective shear modulus for the buckled $\theta=21.8^\circ$. The sinuous character of the $\theta=21.8^\circ$ grain boundary serves as a nucleation point for ripples perpendicular to the grain boundary to form when the supercell is sheared, whereas the single direction of the buckling in $\theta=13.1^\circ$ stabilizes the supercell to ripples perpendicular to the grain boundary. The structure therefore supports the softening that we see in Fig. 4(c).

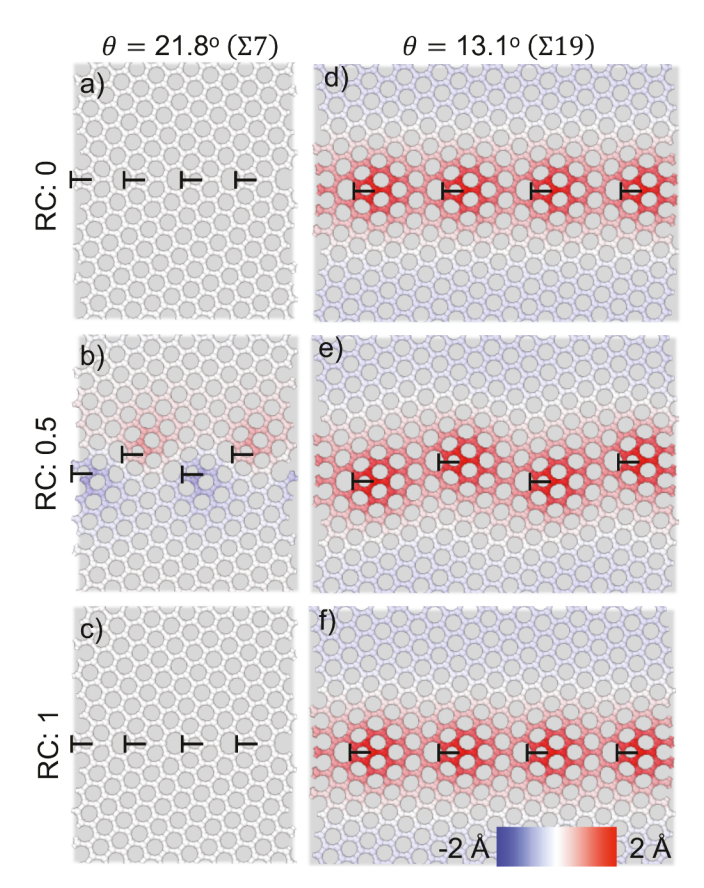


Fig. 5. The structures of buckled $\overline{H}=2$ supercells with (a-c) grain boundary angles of $\theta=21.8^\circ$ (Σ 7), and (d-f) $\theta=13.1^\circ$ (Σ 19). The supercells are repeated twice in the horizontal direction (i.e. 4 dislocations are shown). The out-of-plane deformation is shown using the color bar on the bottom right. (For interpretation of the references to color in this figure legend, the reader is referred to the web version of this article.).

We note that the local out-of-plane deformation is distinct from previously reported wrinkling of pristine graphene that occurs under shear [22]. We find that periodic supercells with grain boundaries also produce such wrinkles. However, in the presence of disconnection induced out-of-plane relaxation, the wrinkling behavior qualitatively changes due to the wrinkle wavelength being pinned by the local out-of-plane relaxation as shown in the SI Section 4. This matches our intuition that the low flexural rigidity of graphene implies that the wrinkle energy is much smaller than the disconnection energies considered here.

4. Discussion and conclusions

The coupling and critical shear analytical models help to form the foundation for conclusions about the mechanisms of shear coupling in graphene. We compare the models directly to atomic scale calculations of shear coupled grain boundary migration across misorientation angles and supercell sizes to show their predictive power. The coupling shear model depends only on the grain boundary topology, implying that the low flexural rigidity of graphene, and likely other 2D materials, does not impact the role that disconnections and shear coupling play as the elementary mechanisms that undergird grain boundary migration. However, as the model formulated for critical shear is sensitive to the disconnection energy and shear modulus, out-of-plane deformation does play a role in the thermodynamic barriers for the intermediate steps of grain boundary migration and could therefore be quite different between different 2D materials, especially those with multiple components (e.g. h-BN). As compared to shear-coupling in bulk materials, the

disconnection cores of 2D materials deform out-of-plane to reduce the shear energy and pin wrinkles.

Despite these differences, the influence of out-of-plane deformation does not affect the principle trends of shear coupling. As seen in Figs. 3 and 4, the flat and buckled graphene sheets have very similar trends, and the differences lie in the particular values of critical shear. Furthermore, we can use the flat supercells as a proxy for the shear coupling of bulk crystals. Since we constrain the supercells to be flat, they are under a plane-strain load similar to that of a bulk crystal with periodic boundary conditions in the z-direction. Therefore, although we show that grain boundary migration in graphene will depend on its environment, out-of-plane deformation seems to be a higher order effect and shear coupling is largely equivalent in 2D and bulk materials.

The dependence of the critical shear on out-of-plane deformation directly impacts the motion of grain boundaries in 2D materials. In particular, our result influences the understanding of the recent observation of h-BN grain boundary sliding due to build-up of shear energy from shear coupling [11]. Namely, the critical shear dependence of out-of-plane deformation is a clear sign that the strain energy is sensitive to the degree of confinement in the out of plane direction. This is of particular importance for the often observed graphene 21° grain boundary [36], for which we observed the most softening in the effective shear modulus. It remains of interest to study the effect of the shear softening when grain boundary motion is activated with increasing temperature. Although temperature will not affect the topological underpinning of shear coupling, the changes in the potential energy surface with confinement may prove insightful into understanding grain boundary evolution and annealing during CVD synthesis.

Declaration of Competing Interest

The authors declare that they have no known competing financial interests or personal relationships that could have appeared to influence the work reported in this paper.

Acknowledgements

EA and EE acknowledge the support of the U.S. National Science Foundation through DMR 1555278 and DMR 1720633. HJ acknowledges support through ARO grant number ARMY W911NF-17-1-0544. BX acknowledges support through the National Center for Supercomputing Applications (NCSA) Students Pushing Innovation (SPIN) program.

Supplementary material

Supplementary material associated with this article can be found, in the online version, at 10.1016/j.actamat.2022.118488

References

- [1] M. Legros, D.S. Gianola, K.J. Hemker, In situ TEM observations of fast grain-boundary motion in stressed nanocrystalline aluminum films, Acta Mater. 56 (14) (2008) 3380–3393, https://doi.org/10.1016/j.actamat.2008.03.032.https://www.sciencedirect.com/science/article/pii/S1359645408002152.
- [2] M. Jin, A. Minor, E. Stach, J. Morris, Direct observation of deformation-induced grain growth during the nanoindentation of ultrafine-grained al at room temperature, Acta Mater. 52 (18) (2004) 5381–5387, https://doi.org/10.1016/j. actamat.2004.07.044.https://www.sciencedirect.com/science/article/pii/S135 9645404004653.
- [3] J. Schfer, K. Albe, Competing deformation mechanisms in nanocrystalline metals and alloys: coupled motion versus grain boundary sliding, Acta Mater. 60 (17) (2012) 6076–6085, https://doi.org/10.1016/j.actamat.2012.07.044.https://www. sciencedirect.com/science/article/pii/S1359645412004922.
- [4] K. Zhang, J.R. Weertman, J.A. Eastman, Rapid stress-driven grain coarsening in nanocrystalline cu at ambient and cryogenic temperatures, Appl. Phys. Lett. 87 (6) (2005) 061921, https://doi.org/10.1063/1.2008377.
- [5] A. Rajabzadeh, M. Legros, N. Combe, F. Mompiou, D. Molodov, Evidence of grain boundary dislocation step motion associated to shear-coupled grain boundary

- migration, Philos. Mag. 93 (10–12) (2013) 1299–1316, https://doi.org/10.1080/14786435.2012.760760.
- [6] J.W. Cahn, Y. Mishin, A. Suzuki, Coupling grain boundary motion to shear deformation, Acta Mater. 54 (19) (2006) 4953–4975, https://doi.org/10.1016/j. actamat.2006.08.004.https://www.sciencedirect.com/science/article/pii/S135 9645406005313.
- M. Velasco, H. Van Swygenhoven, C. Brandl, Coupled grain boundary motion in a nanocrystalline grain boundary network, Scr. Mater. 65 (2) (2011) 151–154, https://doi.org/10.1016/j.scriptamat.2011.03.039.Viewpoint set no. 48: Solid Oxide Fuel Cells
- [8] E.R. Homer, S.M. Foiles, E.A. Holm, D.L. Olmsted, Phenomenology of shear-coupled grain boundary motion in symmetric tilt and general grain boundaries, Acta Mater. 61 (4) (2013) 1048–1060, https://doi.org/10.1016/j.actamat.2012.10.005.https://www.sciencedirect.com/science/article/pii/S135 9645412007306
- [9] L. Wang, Y. Zhang, Z. Zeng, H. Zhou, J. He, P. Liu, M. Chen, J. Han, D.J. Srolovitz, J. Teng, Y. Guo, G. Yang, D. Kong, E. Ma, Y. Hu, B. Yin, X. Huang, Z. Zhang, T. Zhu, X. Han, Tracking the sliding of grain boundaries at the atomic scale, Science 375 (6586) (2022) 1261–1265, https://doi.org/10.1126/science.abm2612.https://www.science.org/doi/abs/10.1126/science.abm2612.
- [10] Z. Shand, E. Stach, J.M.K. Wiezorek, J. Knapp, D. Follstaedt, S. Mao, Grain boundary-mediated plasticity in nanocrystalline nickel, Science 305 (5684) (2004) 654–657, https://doi.org/10.1126/science.1098741.https://www.science.or g/doi/10.1126/science.1098741.
- [11] X. Ren, C. Jin, Grain boundary motion in two-dimensional hexagonal boron nitride, ACS Nano 14 (10) (2020) 13512–13523.
- [12] J.W. Cahn, Y. Mishin, A. Suzuki, Duality of dislocation content of grain boundaries, Philos. Mag. 86 (25–26) (2006) 3965–3980, https://doi.org/10.1080/ 14786430500536909.
- [13] J. Hirth, R. Pond, Steps, dislocations and disconnections as interface defects relating to structure and phase transformations, Acta Mater. 44 (12) (1996) 4749–4763, https://doi.org/10.1016/S1359-6454(96)001322.https://www.sciencedirect.com/science/article/pii/S1359645496001322.
- [14] A. Rajabzadeh, F. Mompiou, M. Legros, N. Combe, Elementary mechanisms of shear-coupled grain boundary migration, Phys. Rev. Lett. 110 (2013) 265507, https://doi.org/10.1103/PhysRevLett.110.265507.https://link.aps.org/doi/10.11 03/PhysRevLett.110.265507.
- [15] L. Wan, S. Wang, Shear response of the Σ9 110 221 symmetric tilt grain boundary in fcc metals studied by atomistic simulation methods, Phys. Rev. B 82 (2010) 214112, https://doi.org/10.1103/PhysRevB.82.214112.https://link.aps.org/d oi/10.1103/PhysRevB.82.214112.
- [16] S.L. Thomas, K. Chen, J. Han, P.K. Purohit, D.J. Srolovitz, Reconciling grain growth and shear-coupled grain boundary migration, Nat. Commun. 8 (1) (2017) 1764, https://doi.org/10.1038/s41467-017-01889-3.
- [17] J. Han, S.L. Thomas, D.J. Srolovitz, Grain-boundary kinetics: a unified approach, Prog. Mater. Sci. 98 (2018) 386–476, https://doi.org/10.1016/j. pmatsci.2018.05.004.
- [18] T. Zhao, C. Xu, W. Ma, Z. Liu, T. Zhou, Z. Liu, S. Feng, M. Zhu, N. Kang, D.-M. Sun, H.-M. Cheng, W. Ren, Ultrafast growth of nanocrystalline graphene films by quenching and grain-size-dependent strength and bandgap opening, Nat. Commun. 10 (1) (2019) 4854, https://doi.org/10.1038/s41467-019-12662-z.
- [19] A.V. Tyurnina, H. Okuno, P. Pochet, J. Dijon, Cvd graphene recrystallization as a new route to tune graphene structure and properties, Carbon N Y 102 (2016) 499–505, https://doi.org/10.1016/j.carbon.2016.02.097.http://www.sciencedi rect.com/science/article/pii/S0008622316301865.
- [20] A. Cresti, J. Carrete, H. Okuno, T. Wang, G.K. Madsen, N. Mingo, P. Pochet, Growth, charge and thermal transport of flowered graphene, Carbon N Y 161 (2020) 259–268, https://doi.org/10.1016/j.carbon.2020.01.040.https://www.sciencedirect.com/science/article/pii/S0008622320300403.
- [21] E. Han, J. Yu, E. Annevelink, J. Son, D.A. Kang, K. Watanabe, T. Taniguchi, E. Ertekin, P.Y. Huang, A.M. van der Zande, Ultrasoft slip-mediated bending in fewlayer graphene, Nature Materials 19 (3) (2020) 305–309, https://doi.org/10.1038/ s41563-019-0529-7.https://doi.org/10.1038/s41563-019-0529-7.
- [22] W.H. Duan, K. Gong, Q. Wang, Controlling the formation of wrinkles in a single layer graphene sheet subjected to in-plane shear, Carbon N Y 49 (9) (2011) 3107–3112, https://doi.org/10.1016/j.carbon.2011.03.033.https://www.scienc edirect.com/science/article/pii/S0008622311002247.
- [23] S. Chen, D.C. Chrzan, Continuum theory of dislocations and buckling in graphene, Phys. Rev. B 84 (2011) 214103, https://doi.org/10.1103/PhysRevB.84.214103.htt ps://link.aps.org/doi/10.1103/PhysRevB.84.214103.
- [24] E. Annevelink, E. Ertekin, H.T. Johnson, Grain boundary structure and migration in graphene via the displacement shift complete lattice, Acta Mater. 166 (2019) 67–74, https://doi.org/10.1016/j.actamat.2018.12.030.https://www.sciencedirect.com/science/article/pii/S1359645418309728.
- [25] O.V. Yazyev, S.G. Louie, Topological defects in graphene: dislocations and grain boundaries, Phys. Rev. B 81 (2010) 195420, https://doi.org/10.1103/ PhysRevB.81.195420.https://link.aps.org/doi/10.1103/PhysRevB.81.195420.
- [26] Y. Wei, J. Wu, H. Yin, X. Shi, R. Yang, M. Dresselhaus, The nature of strength enhancement and weakening by pentagon-heptagon defects in graphene, Nat. Mater. 11 (2012) 759EP, https://doi.org/10.1038/nmat3370.
- [27] J. Wang, F. Ma, M. Sun, Graphene, hexagonal boron nitride, and their heterostructures: properties and applications, RSC Adv. 7 (2017) 16801–16822, https://doi.org/10.1039/C7RA00260B.
- [28] S. Kim, E. Annevelink, E. Han, J. Yu, P.Y. Huang, E. Ertekin, A.M. van der Zande, Stochastic stress jumps due to soliton dynamics in two-dimensional van der waals

- interfaces, Nano Lett. 20 (2) (2020) 1201–1207, https://doi.org/10.1021/acs.nanolett.9b04619.PMID: 31944113
- [29] E. Annevelink, H.T. Johnson, E. Ertekin, Pathways to controlled 3d deformation of graphene: manipulating the motion of topological defects, Curr. Opin. Solid State Mater. Sci. 25 (2) (2021) 100893, https://doi.org/10.1016/j.cossms.2020.10893. https://www.sciencedirect.com/science/article/pii/S1359028620300917.
- [30] S. Plimpton, Fast parallel algorithms for short-range molecular dynamics, J. Comput. Phys. 117 (1) (1995) 1–19, https://doi.org/10.1006/jcph.1995.1039. http://www.sciencedirect.com/science/article/pii/S002199918571039X.
- [31] A.C.T. van Duin, S. Dasgupta, F. Lorant, W.A. Goddard, Reaxff: a reactive force field for hydrocarbons, J. Phys. Chem. A 105 (41) (2001) 9396–9409, https://doi. org/10.1021/jp004368u.
- [32] T.P. Senftle, S. Hong, M.M. Islam, S.B. Kylasa, Y. Zheng, Y.K. Shin, C. Junkermeier, R. Engel-Herbert, M.J. Janik, H.M. Aktulga, T. Verstraelen, A. Grama, A.C.T. van Duin, The reaxff reactive force-field: development, applications and future directions, npj Computational Materials 2 (1) (2016) 15011, https://doi.org/10.1038/npjcompumats.2015.11.https://doi.org/10.1038/npjcompumats
- [33] S.G. Srinivasan, A.C.T. van Duin, P. Ganesh, Development of a reaxff potential for carbon condensed phases and its application to the thermal fragmentation of a large fullerene, J. Phys. Chem. A 119 (4) (2015) 571–580, https://doi.org/ 10.1021/jp510274e.PMID: 25562718
- [34] G. Henkelman, H. Jnsson, Improved tangent estimate in the nudged elastic band method for finding minimum energy paths and saddle points, J. Chem. Phys. 113 (22) (2000) 9978–9985, https://doi.org/10.1063/1.1323224.
- [35] G. Henkelman, B.P. Uberuaga, H. Jnsson, A climbing image nudged elastic band method for finding saddle points and minimum energy paths, J. Chem. Phys. 113 (22) (2000) 9901–9904, https://doi.org/10.1063/1.1329672.
- [36] C. Ophus, A. Shekhawat, H. Rasool, A. Zettl, Large-scale experimental and theoretical study of graphene grain boundary structures, Phys. Rev. B 92 (2015) 205402, https://doi.org/10.1103/PhysRevB.92.205402.
- [37] A. Shekhawat, C. Ophus, R.O. Ritchie, A generalized read-shockley model and large scale simulations for the energy and structure of graphene grain boundaries, RSC Adv. 6 (2016) 44489–44497, https://doi.org/10.1039/C6RA07584C.

- [38] E. Bitzek, P. Koskinen, F. Gähler, M. Moseler, P. Gumbsch, Structural relaxation made simple, Phys. Rev. Lett. 97 (2006) 170201, https://doi.org/10.1103/ PhysRevLett.97.170201.
- [39] K. Tserpes, P. Papanikos, The effect of stone wales defect on the tensile behavior and fracture of single-walled carbon nanotubes, Compos. Struct. 79 (4) (2007) 581–589, https://doi.org/10.1016/j.compstruct.2006.02.020.https://www.sciencedirect.com/science/article/pii/S0263822306000663.
- [40] E. Ertekin, D.C. Chrzan, M.S. Daw, Topological description of the stone-wales defect formation energy in carbon nanotubes and graphene, Phys. Rev. B 79 (2009) 155421, https://doi.org/10.1103/PhysRevB.79.155421.https://link.aps.org/d oi/10.1103/PhysRevB.79.155421.
- [41] J. Han, D.J. Srolovitz, M. Salvalaglio, Disconnection-mediated migration of interfaces in microstructures: i. continuum model, Acta Mater. (2021) 117178, https://doi.org/10.1016/j.actamat.2021.117178.https://www.sciencedirect.com/ science/article/pii/S1359645421005589.
- [42] K.D. Molodov, D.A. Molodov, Grain boundary mediated plasticity: on the evaluation of grain boundary migration - shear coupling, Acta Mater. 153 (2018) 336–353, https://doi.org/10.1016/j.actamat.2018.04.057.https://www.sciencedirect.com/science/article/pii/S1359645418303422.
- [43] K. Chen, J. Han, S.L. Thomas, D.J. Srolovitz, Grain boundary shear coupling is not a grain boundary property, Acta Mater. 167 (2019) 241–247, https://doi.org/ 10.1016/j.actamat.2019.01.040.https://www.sciencedirect.com/science/article/ pii/S1359645419300552.
- [44] N. Combe, F. Mompiou, M. Legros, Multiple coupling modes to relax shear strain during grain boundary migration, Acta Mater. 218 (2021) 117222, https://doi. org/10.1016/j.actamat.2021.117222.https://www.sciencedirect.com/science/ article/pii/S1359645421006029.
- [45] D. Warrington, P. Bufalini, The coincidence site lattice and grain boundaries, Scr. Metall. 5 (9) (1971) 771–776, https://doi.org/10.1016/0036-9748(71)90161-X. http://www.sciencedirect.com/science/article/pii/003697487190161X.
- [46] H. WARRINGTOND, The coincidence site lattice (csl) and grain boundary (dsc) dislocations for the hexagonal lattice, J. Phys. Colloques 36 (1975), C4–87–C4–95, https://doi.org/10.1051/jphyscol:1975410.https://doi.org/10.1051/jphyscol:1975410.